Available online at www.sciencedirect.com
ScienceDirect
Trans. Nonferrous Met. Soc. China 31(2021) 3039−3049
Transactions of Nonferrous Metals Society of China
www.tnmsc.cn

Effects of Fe content on microstructure and properties of Cu−Fe alloy

Meng WANG[1], Qian-ru YANG [1], Yan-bin JIANG[1,2], Zhou LI[1,3],
Zhu XIAO[1,2], Shen GONG[1,2], Yong-ru WANG[4], Chuang-li GUO[5], Hai-gen WEI[6]

1. School of Materials Science and Engineering, Central South University, Changsha 410083, China;
2. Key Laboratory of Non-ferrous Metal Materials Science and Engineering, Ministry of Education, Central South University, Changsha 410083, China;
3. State Key Laboratory of Powder Metallurgy, Central South University, Changsha 410083, China;
4. Ningbo Jintian Copper (Group) Co., Ltd., Ningbo 315031, China;
5. Sirui Advanced Copper Alloy Co., Ltd., Xi'an 710077, China;
6. Faculty of Materials Metallurgy and Chemistry, Jiangxi University of Science and Technology, Ganzhou 341000, China

Received 29 December 2020; accepted 23 July 2021

Abstract: Cu−Fe alloys with different Fe contents were prepared by vacuum hot pressing. After hot rolling and aging treatment, the effects of Fe content on microstructure, mechanical properties and electrical conductivity of Cu−Fe alloys were studied. The results show that, when w(Fe)<60%, the dynamic recrystallization extent of both Cu phase and Fe phase increases. When w(Fe)≥60%, Cu phase is uniformly distributed into the Fe phase and the deformation of alloy is more uniform. With the increase of the Fe content, the tensile strength of Cu−5wt.%Fe alloy increases from 305 MPa to 736 MPa of Cu−70wt.%Fe alloy, the elongation decreases from 23% to 17% and the electrical conductivity decreases from 31%IACS to 19%IACS. These results provide a guidance for the composition and processing design of Cu−Fe alloys.

Key words: Cu−Fe alloy; microstructure; properties; powder metallurgy

1 Introduction

Cu−Fe alloys have the advantages of high electrical conductivity and thermal conductivity of Cu, soft magnetism, high strength and stiffness of Fe [1,2]. Among them, Cu−Fe alloys with low Fe content (<2wt.%) are widely used in lead frame materials, especially the Cu−Fe−P alloy has a mature commercial brand (C19700) [3,4]. Cu−5wt.%Fe alloy and Cu−10wt.%Fe alloy have higher strength and conductivity than those of C5191 (Tin bronze) [5,6]. For Cu−Fe alloys with Fe content higher than 20 wt.%, due to the magnetic shielding properties of Fe, they have great potential in the field of marine communication. When Fe content is higher than 30 wt.%, the alloys obtain good electromagnetic shielding performance and wear resistance [7], and are widely used in cooling plate of communication equipment, electromagnetic shielding system, etc.

As a typical kind of metastable immiscible alloy, Cu−Fe alloys will form two liquid regions during solidification, namely, Cu-rich zone (L1) and Fe-rich zone (L2) [8]. This will result in serious macro-segregation and inhomogeneity in composition, microstructure, and properties of Cu−Fe alloys after solidification [6,9,10]. Especially

Corresponding author: Yan-bin JIANG, Tel: +86-731-88830264, E-mail: jiangyanbin@tsinghua.org.cn;
Zhou LI, Tel: +86-731-88830264, E-mail: lizhou6931@163.com
DOI: 10.1016/S1003-6326(21)65713-8

in the traditional casting process, when the Fe content exceeds 20 wt.%, the macro-segregation of Fe phase is more serious. Some results show that the liquid phase separation of Cu−Fe binary system begins only 20 °C below the equilibrium liquidus [11,12]. To solve the above problems, Cu−Fe alloys with uniform composition and structure can be prepared by powder metallurgy [13,14]. Firstly, Cu powder and Fe powder or Cu−Fe alloy powder were mixed evenly, and then Cu−Fe alloys were prepared by vacuum hot pressing sintering process. It is not necessary to melt the alloys in the technical preparation process. At the same time, it is difficult for Fe to diffuse into Cu at low temperature, so it can effectively restrain the influence of Fe atoms on the electrical conductivity of the alloy. What's more, hot pressing sintering in vacuum can effectively avoid impurities and oxidation problems in the alloys. Besides, by adjusting the volume fraction of Fe phase in the alloys, the plastic flow behavior, microstructure evolution, and properties during the heat treatment can be controlled [15]. SHI et al [16] found that when the mass ratio of Fe: Cu is 7:3, the alloy had the best performance of 1200 MPa and HRB 98. Their research is mainly used in diamond cemented carbide tools; however, the conductivity of the alloy is not considered.

In this work, Cu−70wt.%Fe alloy powder and Cu powder were used as raw materials to prepare Cu−Fe alloys with different Fe contents by powder metallurgy method. The microstructure and properties of Cu−Fe alloys were studied by adjusting the powder proportion, which provided experimental and theoretical basis for the development of Cu−Fe alloy technology.

2 Experimental

First of all, Cu−70wt.%Fe alloy powder was prepared by atomization method. Cu−70wt.%Fe alloy powder and pure Cu powder with particle size less than 37 μm were screened by 37 μm screen. After mixing the Cu−70wt.%Fe alloy powder and pure Cu powder with different composition ratios, Cu−5wt.%Fe, Cu−10wt.%Fe, Cu−20wt.%Fe, Cu−40wt.%Fe, Cu−60wt.%Fe and Cu−70wt.%Fe alloys were prepared by vacuum hot pressing. The hot pressing temperature was 600 °C, the pressure was 400 MPa, and the holding time was 3 h. Cu−Fe alloys with different compositions were hot rolled. The hot rolling temperature was 500 °C and the deformation was 50%.

The tensile samples of Cu−Fe alloys were processed by wire electrical discharge machining (WEDM). The length, width, and thickness of gauge are 35, 5, and 2 mm, respectively. An MTS universal material testing machine was used to test the mechanical properties of alloy samples with different compositions. The tensile strain rate of the samples at room temperature was 10^{-2} mm/s^{-1}. Three samples were tested in each group, and the average value of the test results was taken.

Specimens with size of 50 mm (length) × 5 mm (width) × 2 mm (thickness) were cut from alloy samples with different Fe contents. The resistivity in different states was measured by double-bridge method. Three specimens in each group were tested, and the average value was used to calculate the conductivity.

Specimens of 5 mm (length) × 5 mm (width) × 2 mm (thickness) were cut from alloy samples with different Fe contents. After mechanical polishing and vibration polishing, the specimens were analyzed by electron backscatter diffraction (EBSD). A Tescan mira3 field emission scanning microscope was used for electron microscopy and EBSD. And electron probe micro-analysis (EPMA, JXA−8800R, JEOL, Japan) equipped with OXFORD INCA 500 wavelength dispersive X-ray spectrometer (WDS) was used to determine the distribution of elements. The detection plane was the longitudinal section of the strip to obtain more accurate information of microstructure evolution.

3 Results

3.1 Microstructure of Cu−Fe alloy

Figure 1 shows the SEM images of Cu−*x*wt.%Fe (*x*=5, 10, 20, 40, 60, 70) alloys prepared by powder metallurgy. The microstructure of the alloys consists of Fe phase in dark gray region and Cu phase in light gray region. The circular Fe phase is uniformly distributed in the Cu phase, and the average size is approximately 30 μm. The size and morphology of the original Cu−70wt.%Fe alloy powder particles are retained. The Cu phase is filled in the gap between Cu−70wt.%Fe alloy powders. In addition, most of the sintering defects exist at the interface between Cu and Fe, as shown in the black area. With the increase of Fe content, the amount of

Fe phase increases. When the Fe content is increased to 70 wt.%, the Cu−Fe alloys prepared from Cu−70wt.%Fe alloy powder obtain a more uniform structure.

To further analyze the distribution of Fe in the alloy, the Cu phase and Fe phase in Cu−20wt.%Fe alloy were analyzed by EPMA, as shown in Fig. 2. Figure 2(a) represents the backscattered electron

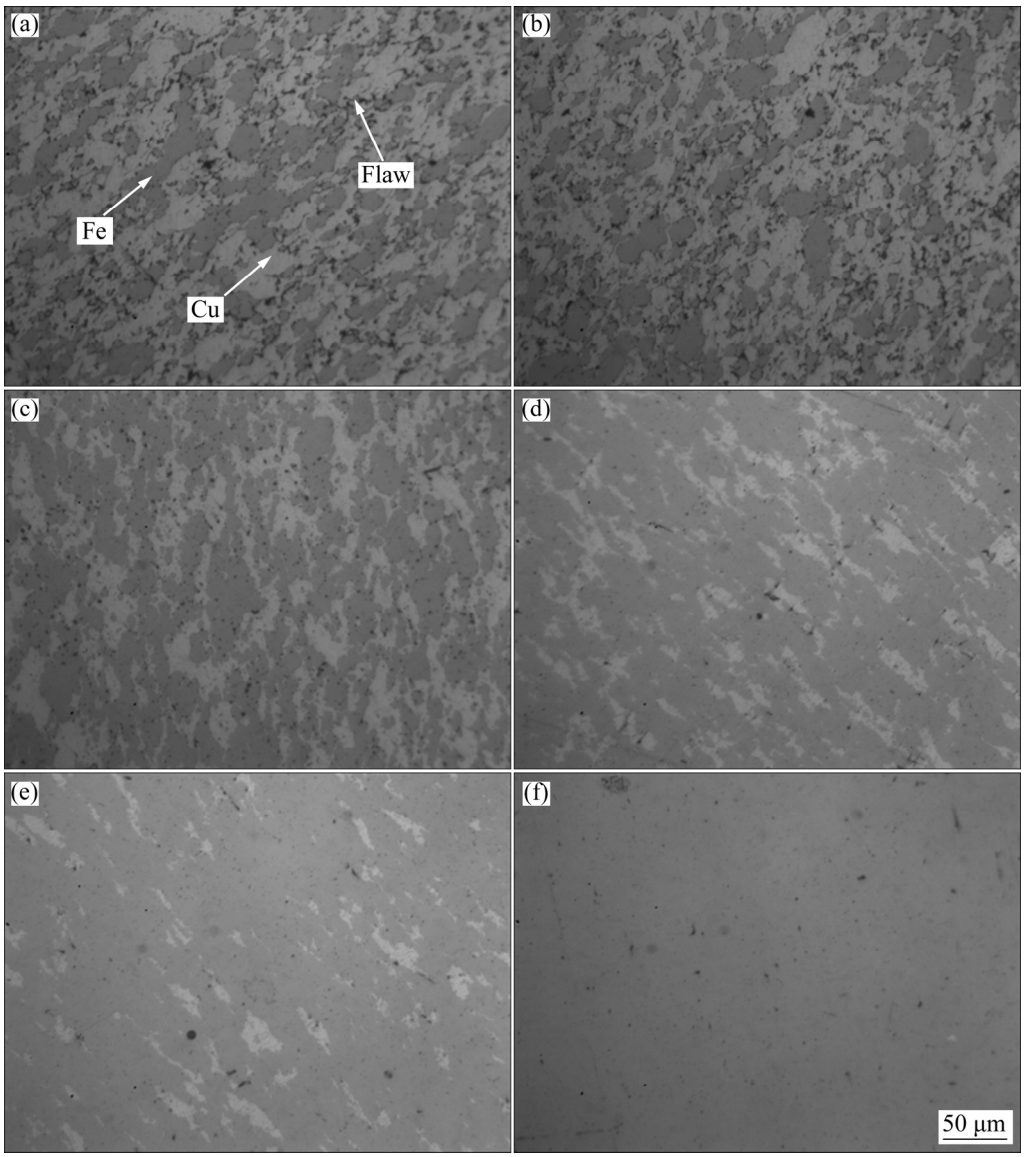

Fig. 1 Microstructures of Cu−Fe alloy with different Fe contents prepared by powder metallurgy: (a) 5wt.%; (b) 10wt.%; (c) 20wt.%; (d) 40wt.%; (e) 60wt.%; (f) 70wt.%

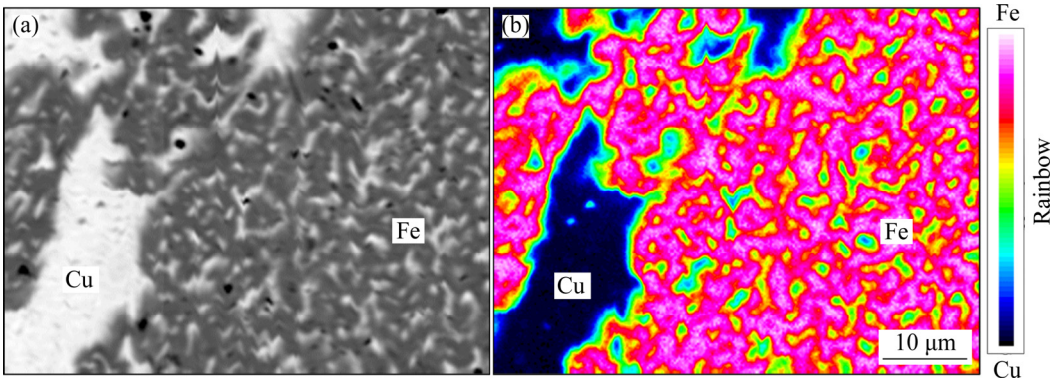

Fig. 2 EPMA of Cu−20wt.%Fe alloy: (a) Backscattered electron image; (b) Element distribution map

image of the alloy, and Fig. 2(b) displays the element distribution map of the corresponding region, and the right side shows the rainbow diagram of the corresponding element content. The gray area in Fig. 2(a) is Fe phase, and Cu-rich zone with a size approximately 1 μm can be observed in the middle of Fe phase [17]. According to the rainbow diagram, the dark blue area is the area with higher Cu contents (Cu content is 80−100 wt.%, 77.82−100 at.%), and the red area is the area with higher Fe contents (Fe content is 70−100 wt.%, 72.64−100 at.%). The Fe content in the green zone is 30−40 wt.% (32.78−43.14 at.%), which indicates that there is a certain degree of mutual diffusion of elements in Cu−Fe alloys during hot pressing, forming a certain degree of metallurgical bonding.

To eliminate the defects in Cu−Fe alloys, the hot rolling process was carried out on the Cu−Fe alloys. The hot rolling temperature was 500 °C and the deformation was 50%. Figure 3 shows the SEM images of Cu−Fe alloys after hot rolling. It can be noticed that the defects at the interfaces between Cu phase and Fe phase in the alloys disappear, indicating that hot rolling can effectively eliminate the sintering defects of the alloys (compare Figs. 3(a−c) and Figs. 1(a−c)).

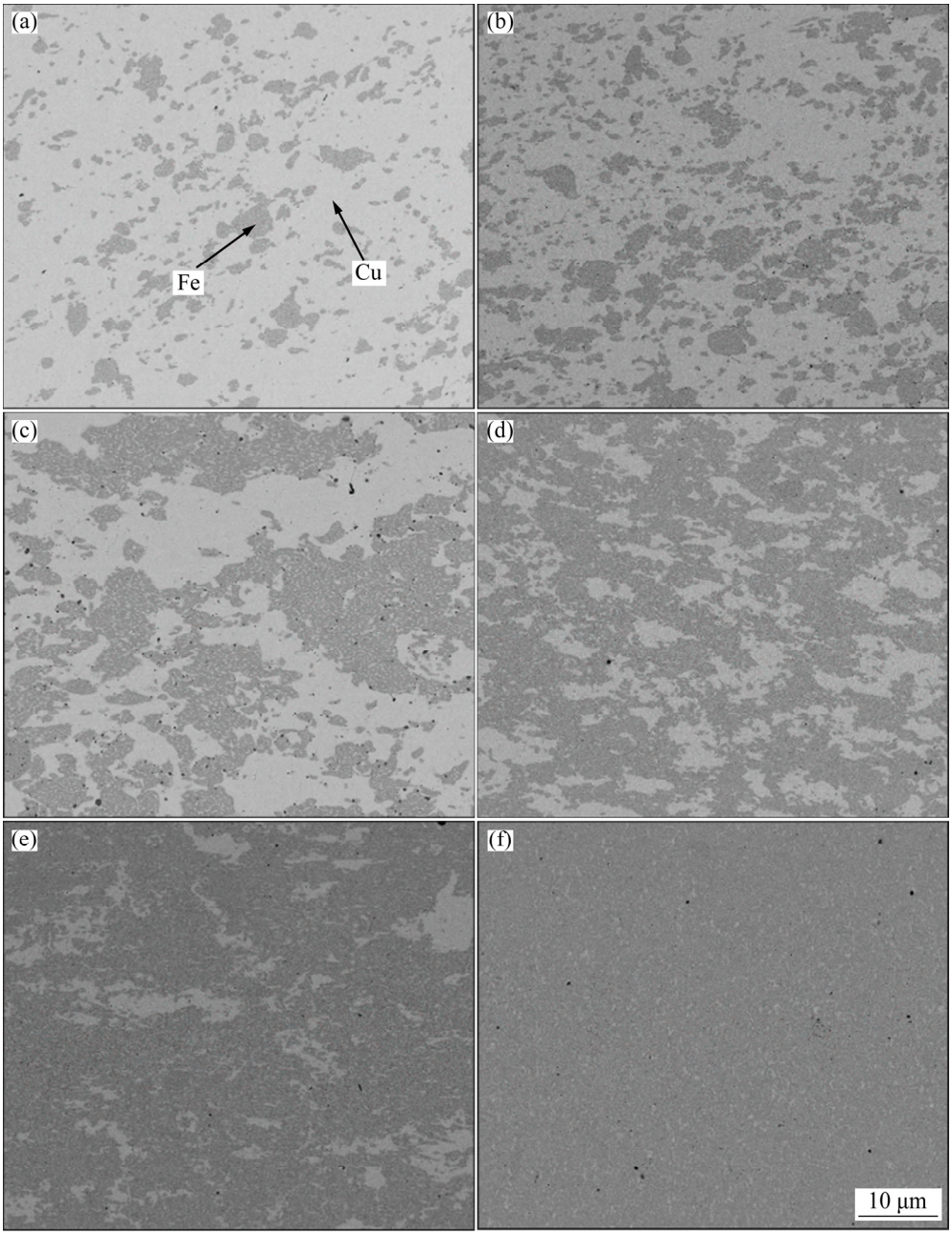

Fig.3 Microstructures of Cu−Fe alloys with different Fe contents after hot rolling: (a) 5 wt.%; (b) 10 wt.%; (c) 20 wt.%; (d) 40 wt.%; (e) 60 wt.%; (f) 70 wt.%

To further study the effect of Fe content on the microstructure of Cu−Fe alloys, EBSD was used to analyze the microstructure of Cu−Fe alloys after hot rolling, as shown in Figs. 4−9. In Figs. 4−9, (b) and (d) display the microstructure of Cu phases, and (c) and (e) show the microstructure of Fe phases. Precisely, (b) and (c) are the dynamic recrystallization distribution of Cu phases and Fe phases, respectively, where the red area is the deformed structure and the yellow area is the sub-grain structure. Besides, the blue area suggests the dynamic recrystallization structure. (d) and (e) in Figs. 4−9 are the inverse pole diagrams (IPF) of Cu phase and Fe phase, respectively. In addition, the black thick lines are large angle grain boundaries (>15°), and the black thin lines are small angle grain boundaries (2°−15°).

Figure 4 shows the EBSD structure of Cu−5wt.%Fe alloy. It can be seen that most areas in the alloy are Cu phase with less Fe phase. Additionally, there are some fine Cu phase particles in the Fe phase (yellow region). It can be observed from Figs. 4(b) and (c) that most of the Cu phase and Fe phase in the hot-rolled Cu−5wt.%Fe alloy are of sub-crystalline structure, and a small amount of dynamic recrystallization structure exists in the

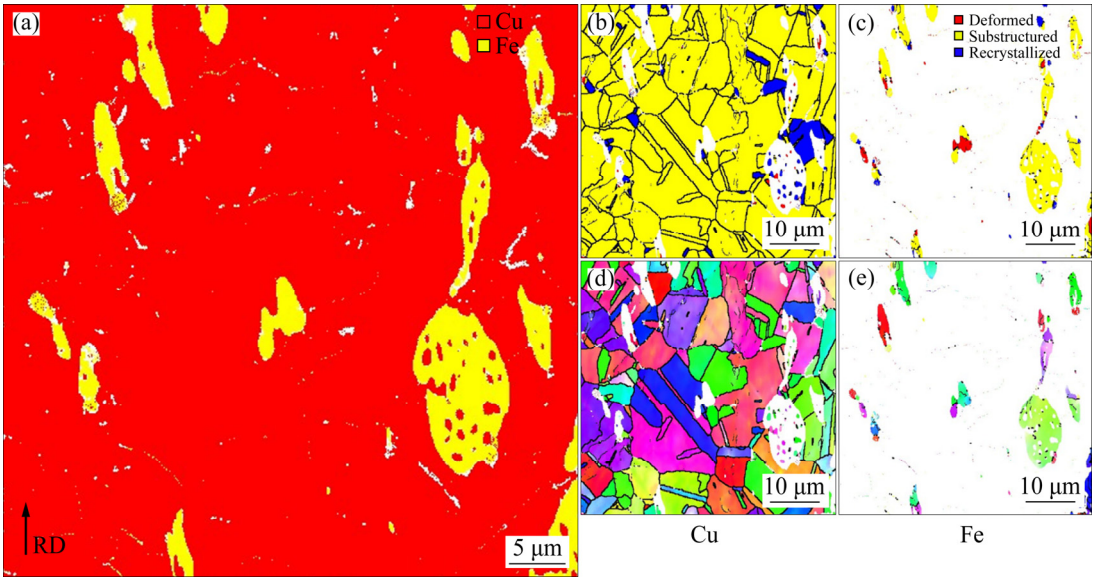

Fig. 4 EBSD images of hot-rolled Cu−5wt.%Fe alloy: (a) Phase distribution diagram; (b) Recrystallization distribution of Cu phase; (c) Recrystallization distribution of Fe phase; (d) IPF of Cu phase; (e) IPF of Fe phase

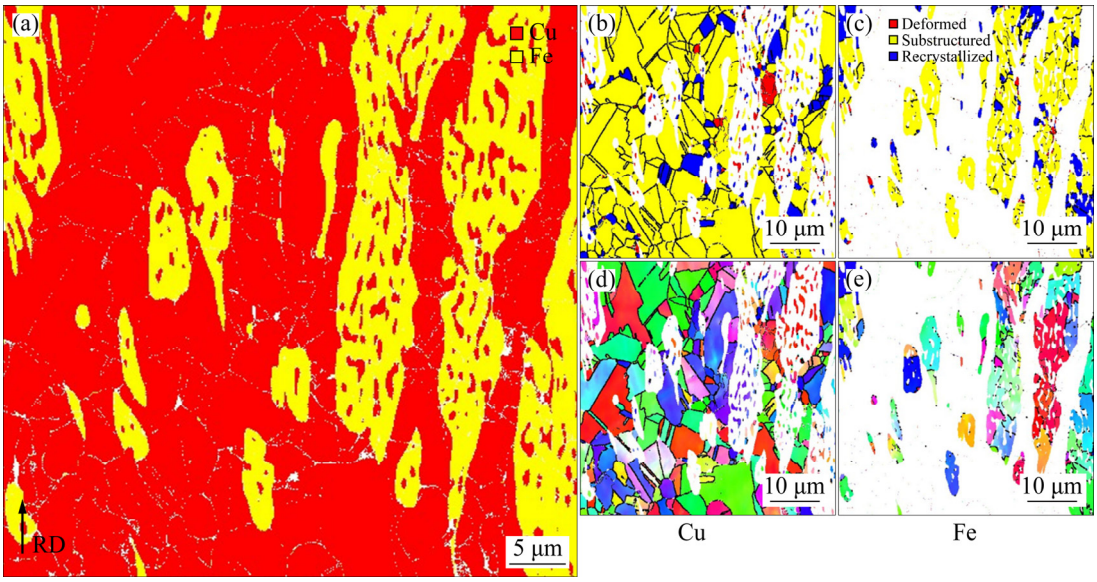

Fig. 5 EBSD images of hot-rolled Cu−10wt.%Fe alloy: (a) Phase distribution diagram; (b) Recrystallization distribution of Cu phase; (c) Recrystallization distribution of Fe phase; (d) IPF of Cu phase; (e) IPF of Fe phase

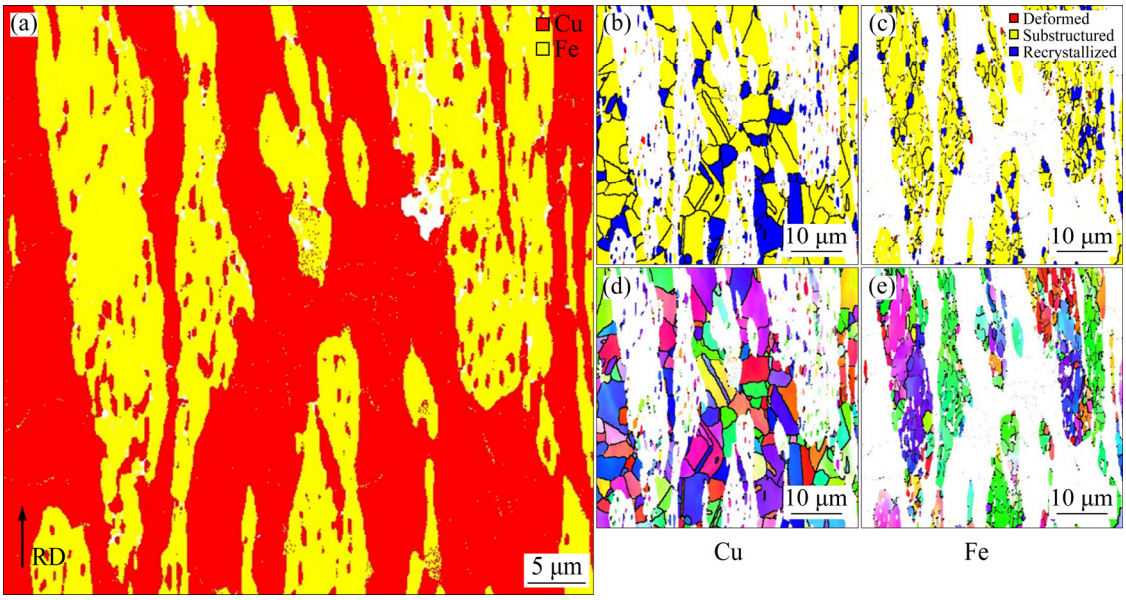

Fig. 6 EBSD images of hot-rolled Cu−20wt.%Fe alloy: (a) Phase distribution diagram; (b) Recrystallization distribution of Cu phase; (c) Recrystallization distribution of Fe phase; (d) IPF of Cu phase; (e) IPF of Fe phase

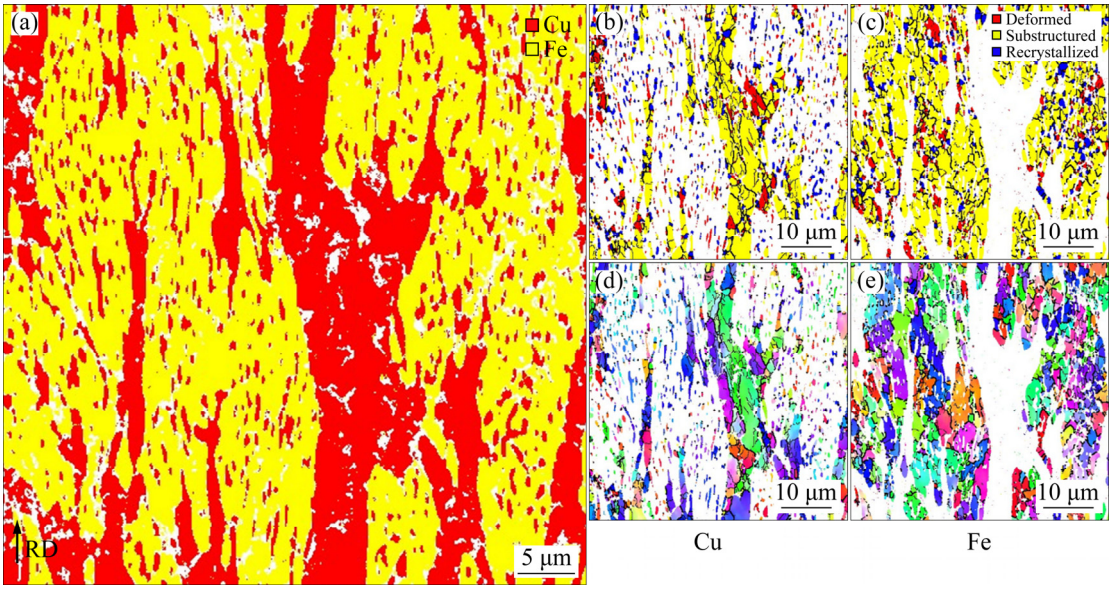

Fig. 7 EBSD images of hot-rolled Cu−40wt.%Fe alloy: (a) Phase distribution diagram; (b) Recrystallization distribution of Cu phase; (c) Recrystallization distribution of Fe phase; (d) IPF of Cu phase; (e) IPF of Fe phase

Cu phase. Figures 4(d) and (e) are the IPF of Cu phase and Fe phase in the alloy, respectively. It can be found from the figure that some twins are produced in the Cu phase, and the average grain size is approximately 12 μm. The grain orientation of Fe phase is basically consistent, which indicates that the deformation degree of Fe phase in the alloy is small.

Figure 5 shows the EBSD structure of Cu−10wt.%Fe alloy. The amount of Fe phase in the alloy increases and it is elongated along the rolling direction. According to Figs. 5(b) and (c), the deformation degree of Fe phase of Cu−10wt.%Fe alloy is significantly higher than that of Cu−5wt.%Fe alloy, and the dynamic recrystallization grain fraction also rises significantly. It can be seen from Figs. 5(d) and (e) that the average grain size of Cu phase is approximately 8 μm, and the average grain size of Fe phase is approximately 6 μm which is smaller than that of Fe phase in Cu−5wt.%Fe alloy. It is also noticed that the grain orientation in Fe phase is more dispersed.

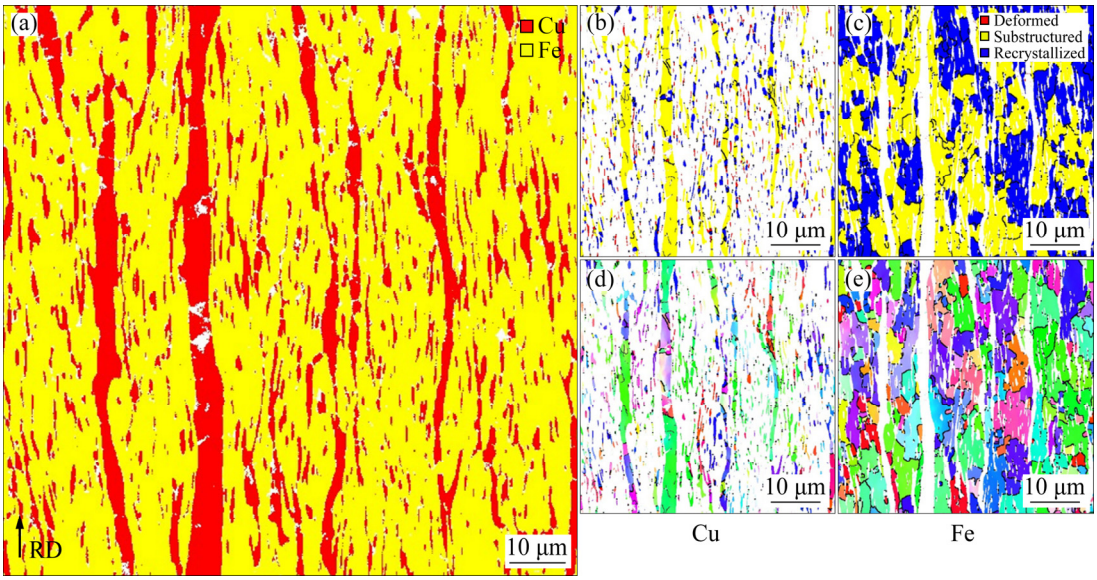

Fig. 8 EBSD images of hot-rolled Cu−60wt.%Fe alloy: (a) Phase distribution diagram; (b) Recrystallization distribution of Cu phase; (c) Recrystallization distribution of Fe phase; (d) IPF of Cu phase; (e) IPF of Fe phase

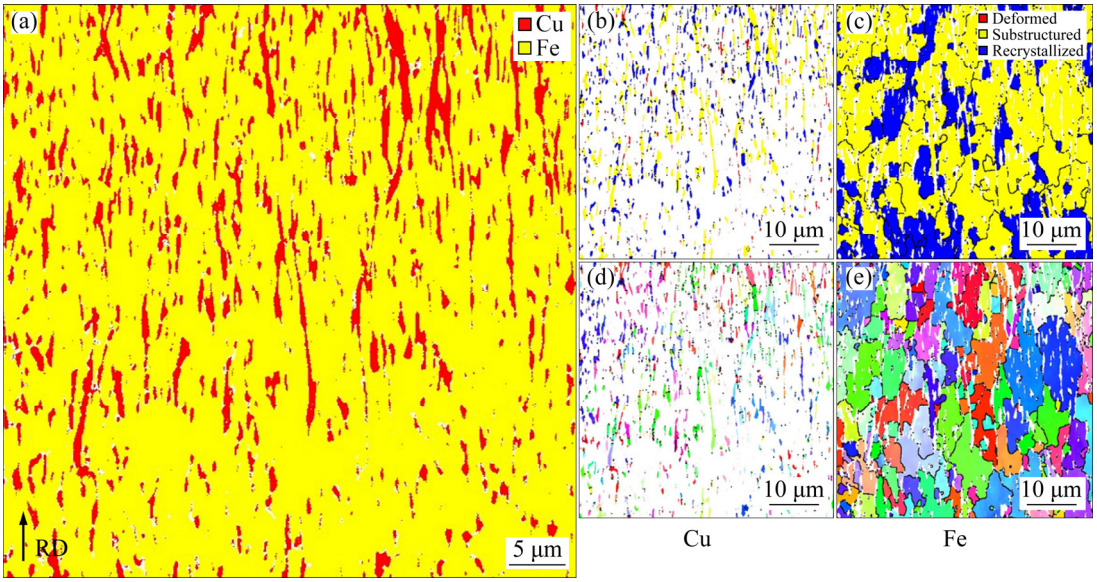

Fig. 9 EBSD images of hot-rolled Cu−70wt.%Fe alloy: (a) Phase distribution diagram; (b) Recrystallization distribution of Cu phase; (c) Recrystallization distribution of Fe phase; (d) IPF of Cu phase; (e) IPF of Fe phase

Figure 6 shows the EBSD structure of Cu−20wt.%Fe alloy. The distribution of Fe phase is similar to that in Cu−10wt.%Fe alloy. It can be seen from Figs. 6(b) and (c) that almost all Cu and Fe phase grains are sub-crystalline and recrystallized. At the same time, the recrystallized grains of Fe phase are finer, approximately 1 μm, and the average grain size of Cu phase is approximately 7 μm, which indicates that the deformation degree of Fe phase in Cu−20wt.%Fe alloy is further increased under the same hot rolling conditions.

Figure 7 shows the EBSD structure of Cu−40wt.%Fe alloy. As the proportion of Cu−70wt.%Fe alloy powder increases, the contact area between Cu−70wt.%Fe alloy powders increases, and a large area of continuous Fe phase region is formed in the alloy. With respect to Figs. 7(b) and (c), there are a lot of recrystallized grains in both Cu and Fe phases. In addition, Figs. 7(d) and (e) suggest that the Cu and Fe phases are broken up more finely during deformation.

Figure 8 shows the EBSD structure of Cu−60wt.%Fe alloy. The amount of Cu phase in the alloy decreases, while the amount of Fe phase

increases obviously and becomes the main phase composition. After hot rolling, the Cu phase in the alloy is elongated along the rolling direction and becomes a slender fiber structure. The recrystallization degree of Fe phase is also enhanced obviously. The average grain size is approximately 12 μm, and the refining degree is reduced.

Figure 9 shows the EBSD structure of Cu−70wt.%Fe alloy. It can be seen from the figure that the Cu phase particles are evenly distributed in the Fe phase, and part of the Cu phase is elongated into fibrous structure along the rolling direction, as shown in Fig. 9(a). In addition, dynamic recrystallization occurs in most Cu and Fe phases, and the deformation degree of the alloy is uniform, as shown in Figs. 9(b) and (c).

3.2 Mechanical properties and electrical conductivity of Cu−Fe alloys

Figure 10 shows the change of tensile strength of Cu−Fe alloys with Fe content after hot rolling and hot rolling + aging (420 °C, 2 h). It can be seen from the figure that with the increase of Fe content, the tensile strength of hot-rolled alloy increases, from 305 MPa of Cu−5wt.%Fe alloy to 736 MPa of Cu−70wt.%Fe alloy, indicating that Fe content is one of the main factors affecting the tensile strength of the alloys. Additionally, the tensile strength of the alloy is improved after aging for 2 h.

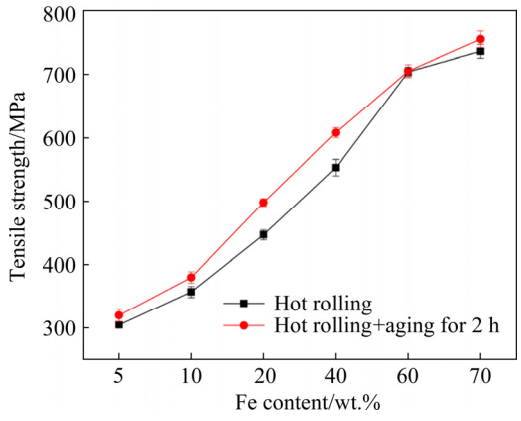

Fig. 10 Tensile strength of Cu−Fe alloys with different Fe contents

Figure 11 shows the change curve of elongation of Cu−Fe alloys with Fe content after hot-rolling and hot-rolling + aging (420 °C, 2 h), respectively. According to Fig. 11, the elongation of the hot-rolled alloys drops with the increase of Fe content. When the Fe content increases to 60 wt.%, the elongation of the alloy reduces from 23% of Cu−5wt.%Fe to 15% of Cu−60wt.%Fe, and the elongation of the alloys slightly increases to 17% when the Fe content continues to increase to 70wt.%. When the Fe content is 5−40 wt.%, the elongation of the alloys after hot rolling and aging treatment is slightly higher than that of the hot-rolled alloys.

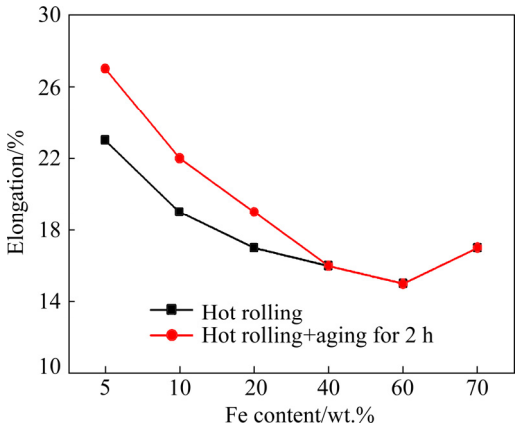

Fig. 11 Variation of elongation of Cu−Fe alloy with Fe content

Figure 12 shows the electrical conductivity of Cu−Fe alloys with Fe content after hot rolling and hot rolling + aging treatment, respectively. With the increase of Fe content, the electrical conductivity of hot-rolled alloys decreases. After aging at 420 °C for 2 h, the electrical conductivity of the alloys increases in varying degrees. For example, the conductivity of Cu−5wt.%Fe alloy increases from 31%IACS to 44%IACS, while that of Cu−70wt.%Fe alloy increases from 14%IACS to 20%IACS.

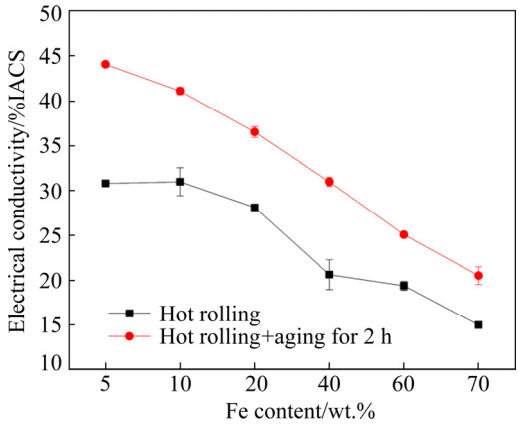

Fig. 12 Variation of electrical conductivity of Cu−Fe alloy with Fe content

4 Discussion

4.1 Effect of Fe content on microstructure of Cu−Fe alloys

According to the results of metallography, EPMA, SEM and EBSD, the microstructure of Cu−Fe alloys during hot rolling is closely related to Fe content. In terms of the difference of Fe content, the microstructure changes of Cu−Fe alloys can be divided into three categories: (1) when the Fe content is less than 20 wt.%, the dynamic recrystallization results in refinement of Cu phase and Fe phase structure, in which Fe phase is elongated into fibrous structure along the rolling direction; (2) when the Fe content is 20−60 wt.%, the dynamic recrystallization degree of Cu phase and Fe phase increases, the grain refinement degree of both phases also increases, and the deformation streamline is more and more obvious; (3) when the Fe content is higher than 60 wt.%, the Cu phase distributes uniformly in the Fe phase, and most of Cu phase and part of Fe phase are recrystallized dynamically, and the deformation of alloy is uniform.

When Fe content is less than 20 wt.%, Cu−Fe alloys consist of Cu phase and honeycomb Fe phase. In the hot rolling process, the yield strength of Cu phase is obviously lower than that of Fe phase [18]. In addition, under the rolling force, Cu phase is more prone to plastic deformation than Fe phase, and the deformation degree of Cu phase is obviously higher than that of Fe phase, which results in larger shear strain at the interface between Cu phase and Fe phase. Under heat and strain, the dynamic recrystallization occurs in Cu phase and Fe phase, and the grains of both phases will be refined. In addition, due to the large particle size of Fe phase (approximately 35 μm), the plastic flow during hot rolling and the shear strain between Cu phase and Fe phase make Fe phase deform along the rolling direction and form fibrous Fe phase structure, as shown in Fig. 5(a).

When the Fe content is 20−60 wt.%, the amount of Fe phase in the alloy rises, and the interfaces between Cu phase and Fe phase also increase. The shear strain of the interfaces between the two phases increases correspondingly, which enhances the dynamic recrystallization of Cu phase and Fe phase obviously, and leads to grain refinement. On the other hand, the hot rolling deformation promotes the grain refinement of Cu and Fe phases, which is more conducive to the thermoplastic flow of Cu and Fe phases, forming deformation streamline structure along the rolling direction, as shown in Fig. 7(a).

When the Fe content is higher than 60 wt.%, the amount of Fe phase in the alloy is larger than that of Cu phase. The soft Cu phase is surrounded by hard Fe phase. During hot rolling, the deformation degree between Cu phase and Fe phase is higher, and the deformation degree is relatively uniform. The shear deformation degree between them is obviously less than that of the alloys with Fe content of 5−40 wt.%. The results suggest that there is less dynamic recrystallization of grains and grain refinement.

4.2 Effect of Fe content on properties of Cu−Fe alloys

The solid solution elements in the alloy matrix remarkably affect the electrical conductivity and mechanical properties of the alloy. From the EPMA result shown in Fig. 2, there is a certain degree of atomic diffusion at the interface between Fe and Cu phases. Therefore, this section discusses the property evolution of the Cu−Fe alloy after hot rolling and hot rolling + aging for 2 h.

(1) Mechanical properties

The effect of Fe content on the mechanical properties of Cu−Fe alloys is closely related to the quantity and microstructure of Cu phase and Fe phase. Under the experimental conditions of this work, Cu−Fe alloys with different compositions (5−70 wt.% Fe) can be considered as composites, whose properties are decided by Fe phase and Cu phase. Fe phase is a hard phase and Cu phase is a soft phase. In the Cu−5wt.%Fe alloy, the minor contribution of Fe to the strength is caused by the small amount of Fe phase and its low deformation degree. Meanwhile, the dynamic recrystallization occurs in the Cu phase. The working hardening of alloy is low, which contributes to a lower strength (305 MPa) and a higher elongation of the alloy (23%). With the increase of Fe content to 60 wt.%, the amount of Fe phase in the alloy increases, and the amount of Cu phase decreases. The increase of hard Fe phase has a greater effect on improving the strength of the alloy than the decrease of soft Cu phase. At the same time, the number of phase

interfaces between Fe phase and Cu phase increases, the dynamic recrystallization of Fe phase and Cu phase increases obviously, and the grain size of both phases is obviously refined. The results show that the strength of the alloy increases with the increase of Fe content. In addition, with the growth of the amount of Fe phase, the hot-rolled work hardening of the alloy is also significantly improved, and the elongation decreases with the increase of Fe content. When the content of Fe is 70 wt.%, the amount of Fe phase continues to increase. The work hardening of the hot rolling alloy also increases, which makes the strength of the alloy continuously increase. Meanwhile, the soft Cu phase distributes evenly in the Fe phase, which makes the elongation increase slightly after fracture of the alloy.

The hot-rolled Cu−Fe alloys with different compositions were aged at 420 °C for 2 h. The Fe atoms which dissolved in Cu phase precipitated and then dispersed as nano-size particles within the Cu phase, leading to the precipitation strengthening effect in a certain degree [13]. Meanwhile, the aging also caused a recovery in the alloy, which reduced dislocations and other defects in Cu phase and Fe phase. However, the effect of precipitation strength of Fe phase is greater than that of recovery softening, which causes slight increase in the strength of alloy (20−50 MPa) and the elongation after fracture.

(2) Electrical conductivity

The influence of the electrical conductivity of Cu−Fe alloys is closely related to the amount of Fe phase and Cu phase, the number of atoms and defects in alloy, and the conductivity of Fe phase is significantly lower than that of Cu phase. For the Cu−Fe alloys, with the increase of Fe content, the amount of Fe phase increases and the amount of Cu phase decreases, which makes the electrical conductivity of the alloy decrease. In addition, the number of Cu/Fe phase interfaces also increases, and the degree of electron scattering increases. Therefore, the increase in Fe phase and Cu/Fe interfaces is the main reason for the decrease of electrical conductivity of Cu−Fe alloy. The hot-rolled Cu−Fe alloys with different compositions were aged at 420 °C for 2 h. The Fe atoms which dissolved in the Cu phase precipitated and the electron scattering decreased, which led to the improvement of electrical conductivity of the alloy after aging.

5 Conclusions

(1) Cu−Fe alloys with different Fe contents were prepared by mechanical mixing and hot pressing with pure Cu powder and Cu−70wt.%Fe alloy powder. After hot rolling at 500 °C and aging at 420 °C for 2 h, the tensile strength, elongation to failure and electrical conductivity of Cu−70wt.%Fe alloy are 755 MPa, 17% and 20%IACS, respectively.

(2) Fe content has a great effect on the microstructure of Cu−Fe alloys. When w(Fe)<60%, the dynamic recrystallization extent of both Cu phase and Fe phase increases, which improves the grain refinement of both phases, and the deformation streamline is more obvious. When w(Fe)≥60%, the Cu phase is more evenly distributed into the Fe phase, and dynamic recrystallization happens in most of Cu phase and part of Fe phase.

(3) With the increase of the Fe content, the tensile strength of Cu−5wt.%Fe alloy increases from 305 MPa to 736 MPa of Cu−70wt.%Fe alloy, the elongation decreases from 23% to 17%, and the electrical conductivity decreases from 31%IACS to 19%IACS.

Acknowledgments

The authors are grateful for the financial supports from the National Natural Science Foundation of China (No. 51974375), Key Project of “Technology Innovation 2025”, Ningbo, China (No. 2018B10030), Technology Research Program of Shenzhen, China (No. JSGG20170824162647398), Project of State Key Laboratory of Powder Metallurgy, Central South University, China, and Young People Fund of Jiangxi province, China (No. 2018BAB216005).

References

[1] LU X P, YAO D W, CHEN Y. Microstructure and hardness of Cu−12%Fe composite at different drawing strains [J]. Journal of Zhejiang University (Science A), 2014, 15: 149−156.

[2] FUNKENBUSCH P D, COURTNEY T H. Microstructural strengthening in cold worked in situ Cu−14.8vol.%Fe composites [J]. Scripta Metallurgica, 1981, 15: 1349−1354.

[3] LU D P, WANG J, ZENG W J, LIU Y, LU L, SUN B D. Study on high-strength and high-conductivity Cu−Fe−P alloys [J]. Materials Science and Engineering A, 2006, 421: 254−259.

[4] DONG Qi-wei, WANG Ming-pu, JIA Yan-lin, XIA Cheng-dong, WANG Wu. Microstructure of as-cast and homogenized Cu−Fe−P−Zn alloy [J]. Journal of Central South University (Science and Technology), 2012(12): 4658−4665. (in Chinese)
[5] HU D C, CHEN M H, WANG L, CHENG H. Dynamic tensile behaviour and deformational mechanism of C5191 phosphor bronze under high strain rates deformation [J]. Materials Science and Engineering A, 2016, 649: 68−73.
[6] WANG M, ZHANG R, XIAO Z, GONG S, JIANG Y B, LI Z. Microstructure and properties of Cu−10wt.%Fe alloy produced by double melt mixed casting and multi-stage thermomechanical treatment [J]. Journal of Alloy and Compounds, 2020, 820: 153323.
[7] JEONG Y B, JO H R, KIM J T, HONG S H, KIM K B. A study on the micro-evolution of mechanical property and microstructures in (Cu−30Fe)−2X alloys with the addition of minor alloying elements [J]. Journal of Alloy and Compounds, 2019, 786: 341−345.
[8] LUO S B, WANG W L, CHANG J, XIA Z C, WEI B. A comparative study of dendritic growth within undercooled liquid pure Fe and Fe50Cu50 alloy [J]. Acta Materialia, 2014, 69: 355−364.
[9] WANG C P, LIU X J. Formation of immiscible alloy powders with egg-type microstructure [J]. Science, 2002, 297: 990−993.
[10] WANG C P, LIU X J, KAINUMA R. Formation of core-type macroscopic morphologies in Cu−Fe base alloys with liquid miscibility gap [J]. Metallurgical & Materials Transactions A, 2004, 35: 1243−1253.
[11] NAKAGAWA Y. Liquid immiscibility in copper-iron and copper-cobalt systems in the supercooled state [J]. Acta Metallurgica, 1958, 6: 704−711.
[12] ANDREW M M, OLUWATOYIN E J, TIMOTHY D B, ROBERT F C. Dynamics of core-shell particle formation in drop-tube processed metastable monotectic alloys [J]. Acta Materialia, 2020, 188: 591−598.
[13] OUYANG Y, GAN X P, ZHANG S Z, LI Z, ZHOU K C, JIANG Y X, ZHANG X W. Age-hardening behavior and microstructure of Cu−15Ni−8Sn−0.3Nb alloy prepared by powder metallurgy and hot extrusion [J]. Transactions of Nonferrous Metals Society of China, 2017, 27: 1947−1955.
[14] TAN L M, WANG Z X, LI Y P, LIU Y, LIU F. Strengthening the bimodal-grained powder metallurgy ferritic steels with Cu addition by aging hardening [J]. Materials Science and Engineering A, 2021, 800: 140312.
[15] WANG M, JIANG Y B, LI Z, XIAO Z, GONG S, QIU W T, LEI Q. Microstructure evolution and deformation behaviour of Cu−10wt%Fe alloy during cold rolling [J]. Materials Science and Engineering A, 2021, 801: 140379.
[16] SHI H C, DUAN L C, TAN S C, FANG X H. Influence of pre-alloying on Fe−Cu based metal matrix composite [J]. Journal of Alloys and Compounds, 2021, 868: 159134.
[17] WANG Y F, AN J, YIN K, WANG M S, LI Y S, HUANG C X. Ultrafine-grained microstructure and improved mechanical behaviors of friction stir welded Cu and Cu−30Zn joints [J]. Materials Science and Engineering A, 2018, 31: 878−886.
[18] MOON J, PARK J M, BAR J W, DO H, LEE B, KIM H S. A new strategy for designing immiscible medium-entropy alloys with excellent tensile properties [J]. Acta Materialia, 2020, 193: 71−82.

Fe 含量对 Cu−Fe 合金组织与性能的影响

王 檬[1]，杨倩如[1]，姜雁斌[1,2]，李 周[1,3]，肖 柱[1,2]，龚 深[1,2]，王永如[4]，郭创立[5]，魏海根[6]

1. 中南大学 材料科学与工程学院，长沙 410083；
2. 中南大学 有色金属材料科学与工程教育部重点实验室, 长沙 410083；
3. 中南大学 粉末冶金国家重点实验室, 长沙 410083；
4. 宁波金田铜业(集团)股份有限公司，宁波 315031；
5. 西安斯瑞先进铜合金科技有限公司，西安 710077；
6. 江西理工大学 材料冶金化学学部，赣州 341000

摘 要：采用真空热压法制备不同 Fe 含量的 Cu−Fe 合金坯料。研究 Fe 含量对热轧和时效处理 Cu−Fe 合金组织、力学性能和导电率的影响规律和机理。结果表明，当 Fe 含量＜60%(质量分数)时，Cu 相和 Fe 相动态再结晶程度增大；当 Fe 含量≥60%时，Cu 相颗粒均匀分布在 Fe 相中，合金变形较均匀。随着 Fe 含量的增加，抗拉强度从 Cu−5%Fe 合金的 305 MPa 增加至 Cu−70%Fe 合金的 736 MPa，其断后伸长率则从 23%下降至 17%，导电率从 31%IACS 下降至 19%IACS。该结果对 Cu−Fe 合金的成分和加工工艺设计具有指导意义。

关键词：Cu−Fe 合金；组织；性能；粉末冶金

(Edited by Xiang-qun LI)